Journal of Hazardous Materials 174 (2010) 598–609

Contents lists available at ScienceDirect

Journal of Hazardous Materials

journal homepage: www.elsevier.com/locate/jhazmat

Comparison of photodegradative efficiencies and mechanisms of Victoria Blue R assisted by Nafion-coated and fluorinated TiO_2 photocatalysts

K.T. Chen[b], C.S. Lu[c], T.H. Chang[b], Y.Y. Lai[d], T.H. Chang[e], C.W. Wu[d], C.C. Chen[a,*]

[a] Department of Science Application and Dissemination, National Taichung University, Taichung 403, Taiwan, ROC
[b] Department of General Education, Ming Hsing University of Science and Technology, 304, Taiwan, ROC
[c] Department of General Education, National Taichung Nursing College, Taichung 403, Taiwan, ROC
[d] Department of Applied Chemistry, Chung-Shan Medical University, Taichung 402, Taiwan, ROC
[e] Department of Electronic Engineering, Ming Hsing University of Science and Technology, 304, Taiwan, ROC

ARTICLE INFO

Article history:
Received 3 April 2009
Received in revised form 26 August 2009
Accepted 17 September 2009
Available online 23 September 2009

Keywords:
Nafion-coated TiO_2
Fluorinated TiO_2
Photocatalytic
Dye
High-performance liquid chromatography–mass spectrometry
Victoria Blue R

ABSTRACT

The purposes of this research were to study the effects of two modified photocatalysts, Nafion-coated TiO_2 and fluorinated TiO_2, and photocatalytic degradation of Victoria Blue R in aqueous solution. Photocatalytic degradation of Victoria Blue R was accelerated by the modified photocatalysts. Bulk and surface characterizations of the resulting powders were carried out. Attachment of the anions to the TiO_2 surface using the Nafion-coated-TiO_2 possibly results in increased adsorption of the cationic dye, and the degradation rate is larger for the cationic dye. It was found that Victoria Blue R on the two illuminated TiO_2 surfaces underwent very different changes. To obtain a better understanding on the mechanistic details of this modified-TiO_2-assisted photodegradation of the Victoria Blue R dye with UV irradiation, a large number of intermediates of the process were separated, identified, and characterized by a high-performance liquid chromatography–mass spectrometry technique. Several probable photodegradation pathways were proposed and discussed.

1. Introduction

Triphenylmethane dyes have been extensively used as textile dyes for wool, silk, and cotton, in the preparation of inks and in the surface-coating and dyeing of paper [1,2], as colorants in foods, drugs, cosmetics [3], as biological stains, and as anti-infective, antimicrobial and antihelmintic agents [1]. The photocytotoxicity of triphenylmethane dyes, based on the production of the reactive oxygen species, is tested intensively with the regard to their photodynamic treatment [4]. An additional worry is that some triphenylmethane dyes have been shown to be potent clastogens, possibly responsible for promoting tumor growth in some species of fish [5]. Doerge et al. [6] have demonstrated that leucomalachite green inhibits thyroid peroxidase-catalyzed formation of thyroxine and tyrosine in vitro, which also results in the oxidative *N*-demethylation of leuco-malachite green to a primary phenylamine. An early report [7,8] describes how the molecular structure of four cationic triphenylmethanes dyes—Victoria Blue R, Victoria Pure Blue BO, Crystal Violet, and Ethyl Violet—affects their efficiency as mediators of the photoinduced inactivation of two model mitochondrial targets, hexokinase and DNA. Hexokinase is known to be over expressed in highly glycolytic tissues such as tumors, and this enzyme has been previously considered as a possible target for anti-tumor therapy. Mitochondrial DNA is particularly prone to oxidative damage due to both its lack of protective histones and proof reading and the presence of incomplete repair mechanisms in the mitochondrial machinery.

The TiO_2-mediated photocatalysis process has been successfully used to degrade pollutants during the past few decade years [9,10]. TiO_2 is broadly used as a photocatalyst because of its non-toxicity, photochemical stability, and low cost [9]. Heterogeneous photocatalysis is an emerging destructive technology which leads to the total mineralization of many dye pollutants through the proposed mechanism [10]. Because the photocatalytic reactions mostly take place on the surface, the surface property of TiO_2 is regarded as one of the most important factors in determining the photocatalytic reaction kinetics and mechanisms. A major limitation of achieving high photocatalytic efficiency in semiconductor systems is the quick recombination of charge carriers. Recombination, which has faster kinetics than surface redox reactions, is a major drawback as it reduces the quantum efficiency of photocatalysis. Therefore, ways to minimize the recombination rate are important if we are interested in maximizing photocatalysis efficiency. For this purpose, TiO_2 has been investigated in relation to

* Corresponding author. Tel.: +886 4 2218 3839; fax: +886 4 2218 3530.
E-mail address: ccchen@ms3.ntcu.edu.tw (C.C. Chen).

0304-3894/$ – see front matter © 2009 Elsevier B.V. All rights reserved.
doi:10.1016/j.jhazmat.2009.09.094

modify (Nafion-coated TiO_2, Nafion-TiO_2) or surface complexation (fluorinated TiO_2, F-TiO_2) [11–18].

It is worth noting that fluorination and Nafion coating have been proposed recently by several groups as a method to improve the photocatalytic activity of TiO_2 [11,19–22]. Significant changes in the photocatalytic behavior of TiO_2 have been evidenced in most cases. The adsorption of fluoride on the TiO_2 surface has been supposed to prevent the generation of surface bound hydroxyls and to enhance the formation of solution hydroxyl radicals. More recently, a few F-doped non-TiO_2 catalysts also exhibited a similar enhancement of photocatalytic activities [23,24]. In a recent study Nafion-TiO_2 films were prepared to modify the surface charge of TiO_2. Nafion (Fig. 1) is an anionic perfluorinated polymer [25] and chemically inert in both oxidative and reductive environments, even under UV illumination [22]. Recently, a few Nafion-coated non-TiO_2 catalysts [26–28] exhibited a similar enhancement of photocatalytic activities.

Studies on photocatalytic degradation using TiO_2 modified with different classes of organics have appeared in the citations above, and most of them include a detailed examination of the so-called primary processes under different working conditions. However, less attention has been paid to the study of the degradation mechanism and to the identification of major transient intermediates, which have been more recently recognized as very important aspects of these processes, especially in view of their practical applications. The main purpose of our work is to compare the mechanisms as well as the photocatalytic reaction efficiency on the surface of the F-TiO_2 and Nafion-TiO_2 catalysts. We report herein that this efficiency may be enhanced by the preparation of Nafion-TiO_2 or F-TiO_2. Bulk and surface characterizations of the resulting powders were carried out by means of field emission scanning electron microscopy (FESEM), X-ray diffraction (XRD), determination of Brunauer–Emmett–Teller (BET) specific surface areas, and porosity measurement techniques. Moreover, Victoria Blue R (VBR) dye was used as a model to examine the activity of the photocatalyst and the mechanisms of photocatalytic degradation. To provide an overall understanding of the reaction pathway(s), high-performance liquid chromatography–photodiode array detection-electrospray ionization-mass spectrometry (HPLC–PDA-ESI-MS) was used to identify the *N*-de-alkylated intermediates and the intermediates of VBR from ring cleavage during the photodegradation. So more information of mechanism and efficiency of photocatalysis will be obtained. This work may provide new insights into the mechanisms of photocatalytic degradation by the F-TiO_2 and Nafion-TiO_2 catalysts, insights that may enable us to design and prepare more efficient photocatalysts.

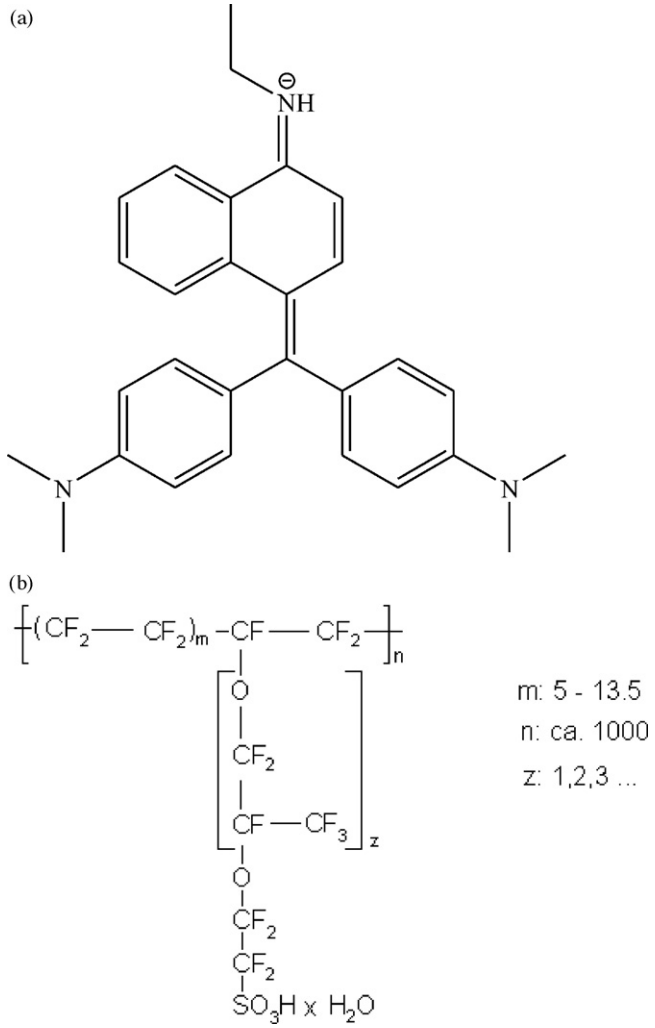

Fig. 1. Chemical structure of (a) VBR and (b) Nafion polymer.

2. Experimental

2.1. Materials and catalysts preparation

Titanium dioxide (P25)—a known mixture of 80% anatase and 20% rutile, with an average particle size of 30 nm, nonporous, and with a reactive surface area of $50 \pm 10\ m^2\ g^{-1}$—was used as-received for all degradation experiments and supplied by Degussa Co. VBR [Bis(4-dimethylaminophenyl)(4-ethylaminonaphthenyl) methylium chloride; Victoria Blue R; C.I. 44040] dye and sodium fluoride were obtained from Sigma–Aldrich and used without any further purification. Nafion was purchased from Aldrich as a 5 wt% solution in a mixture of alcohol and water. The chemical structure of the VBR dye and Nafion is shown in Fig. 1. 4-(*N*-methylaminophenol) (MAP; with a guaranteed purity of 98%) and 4-amioonaphthen-1-ol (purity of 90%) were obtained from Aldrich. 4-aminophenol (AP; analytical standard) was purchased from Riedel-deHaen. The 4-(*N*,*N*-dimethylamino)-4′-(*N*′,*N*′-dimethylamino)benzophenone was obtained from Acros Organics. Reagent-grade ammonium acetate, sodium hydroxide, nitric acid, and HPLC-grade methanol were purchased from Merck. De-ionized water was used throughout this study. The water was then purified with a Milli-Q water ion-exchange system (Millipore Co.) to give a resistivity of 18 MΩ cm.

The Nafion-TiO_2 catalyst was prepared as described elsewhere [18]. The Nafion-coated TiO_2 samples were prepared by adding the desired amount of Nafion solution (5 wt%) to 1 g of TiO_2 along with an appropriate amount of methanol for proper mixing and to ensure a homogeneous coating of Nafion onto TiO_2. After being mixed manually, the mixture was dried overnight at room temperature. The F-TiO_2 catalyst was prepared as described elsewhere [16]. Sodium fluoride (NaF) was added to aqueous TiO_2 suspensions to fluorinate the TiO_2 surface. For the surface analysis of F-TiO_2, TiO_2 suspension (1 g/L) with 10 and 20 mM NaF at pH 4 was filtered through a 0.45 μm filter and dried at 95 °C overnight.

2.2. Photocatalytic experiments

The schematic of diagram of experimental apparatus was shown in our early report [29]. The C-75 Chromato-Vue cabinet of UVP provides a wide area of illumination from the 15-W UV-365 nm tubes (Hitachi) positioned on two sides of the cabinet interior. The photocatalytic activities of the as-prepared samples for the degradation of VBR in solution were tested under UV-365 nm light irradiation (15 W). In a 100 mL suspension containing 50 mg L^{-1}

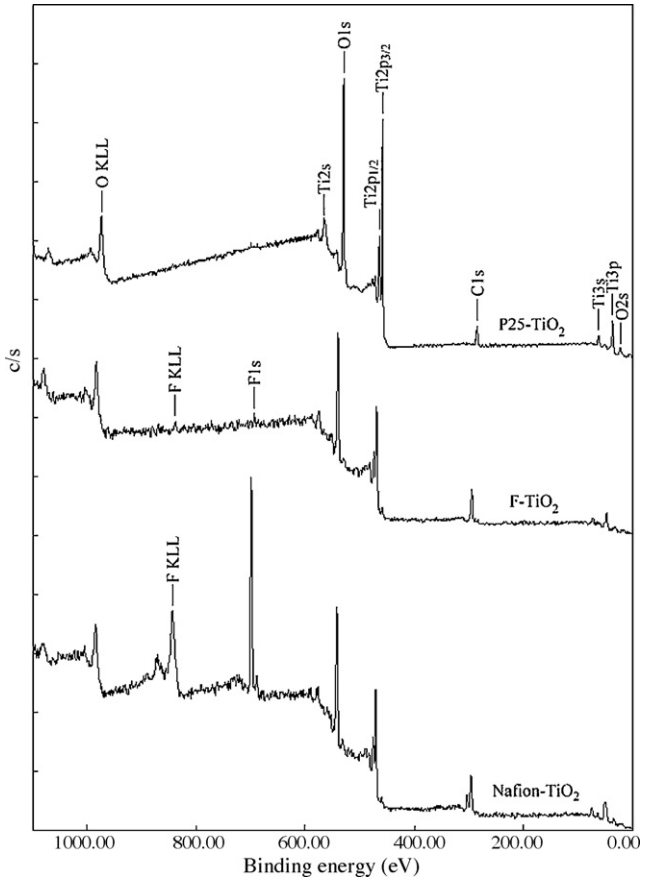

Fig. 2. XPS survey spectrum of P25-TiO_2, F-TiO_2 and Nafion-TiO_2 catalysts prepared.

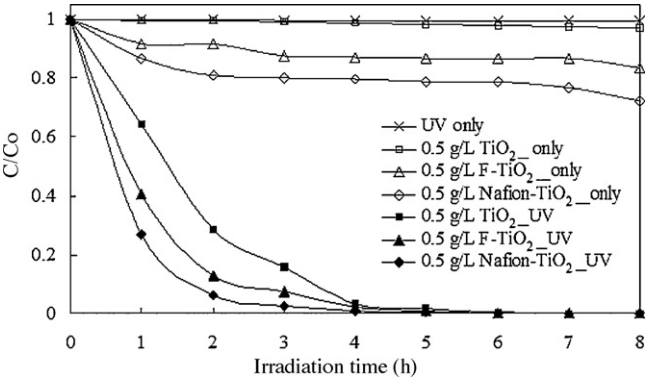

Fig. 3. The photolysis, adsorption and photodegradation rate of VBR with catalysts at pH 9, catalyst = 0.5 g L^{-1}, VBR = 0.05 g L^{-1}.

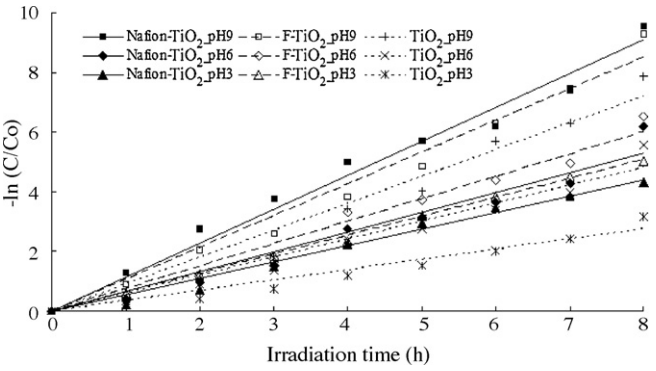

Fig. 4. The pH effect on the VBR photodegradation rate with concentrations of catalysts (0.5 g L^{-1}) and VBR dye (0.05 g L^{-1}).

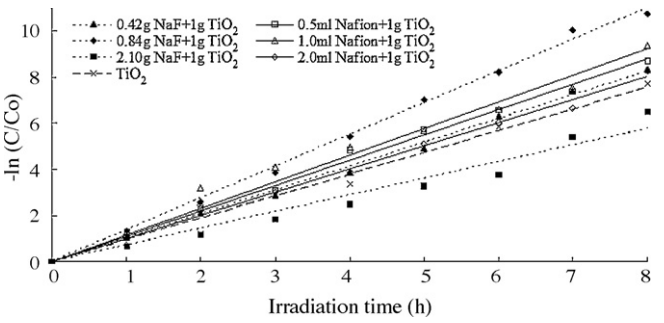

Fig. 5. Influence of the addition ratio in synthesis catalysts on the photodegradation rate for the decomposition of VBR at pH 9, catalysts = 0.5 g L^{-1}, VBR = 0.05 g L^{-1}.

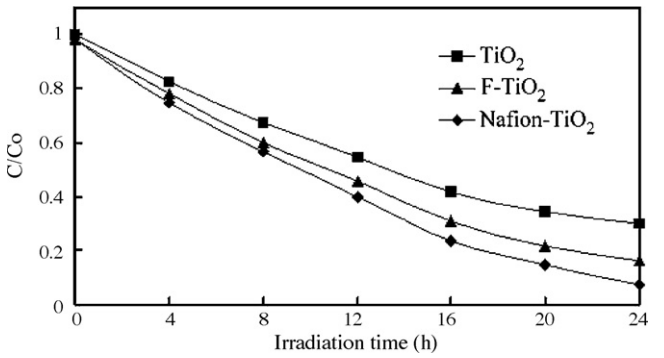

Fig. 6. Depletion in TOC as a function of irradiation time for an aqueous solution of VBR in the presence of F-TiO_2. Experimental condition: dye concentration (0.05 g L^{-1}), F-TiO_2 (0.5 g L^{-1}), pH 9, continuous.

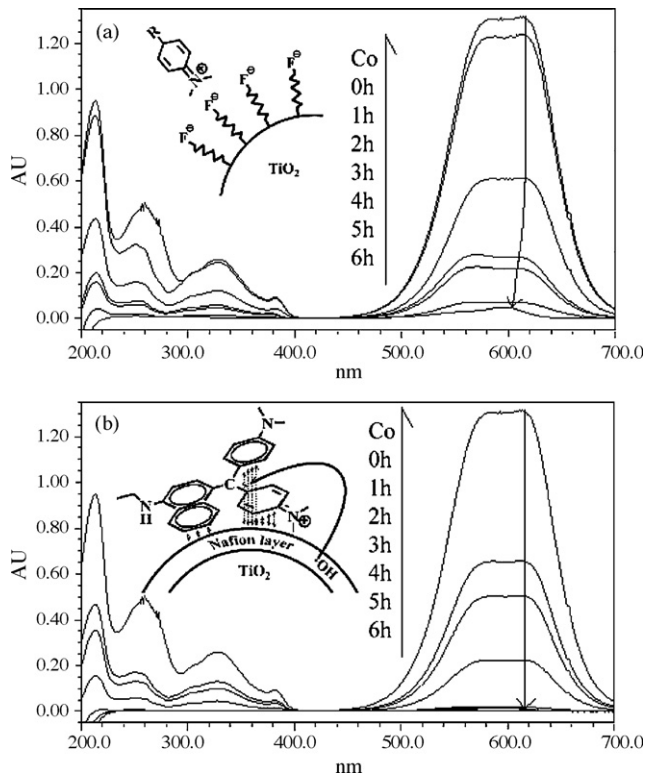

Fig. 7. UV–vis spectra changes of the VBR dye in aqueous at pH 9, with (a) F-TiO_2 and (b) Nafion-TiO_2.

VBR dye, 0.1, 0.5, or 1.0 g L^{-1} of the catalysts was dispersed in a 100 mL flask. For reactions in different pH media, the initial pH of the suspensions was adjusted by addition of either NaOH or HNO_3 solutions. Prior to irradiation, the suspensions were magnetically stirred in the dark for 2 h to ensure the establishment of an adsorption–desorption equilibrium. The suspensions were kept under constant air-equilibrated conditions before and during the irradiation. At given time intervals, 5 mL aliquots were sampled and centrifugated to remove the particles. The filtrates were analyzed by HPLC–PDA-ESI-MS. Performed in flask without addition of modified-TiO_2, the blank experiments showed no appreciable decolorization of the irradiated solution, and thus confirmed the expected stability of this VBR dye under UV light irradiation. Also with addition of 0.5 g L^{-1} modified-TiO_2 to solutions, which contained 50 mg L^{-1} of the VBR dye, the dye remained stable in the dark too.

2.3. Instruments and analytical methods

2.3.1. Characterization

X-ray powder diffraction (XRD) patterns were recorded on a MAC Sience, MXP18 X-ray diffractometer with Cu Kα radiation (λ = 1.54178 Å), operated at 40 kV and 80 mA. Field emission scanning electron microscopy (FESEM) measurement was carried out with a field-emission microscope (JEOL JSM-7401F or JSM-6330F) operated at an acceleration voltage of 15 kV. For the surface analysis, pelletized to thin disks with a high-pressure pelletizer. These pellets were analyzed with high resolution X-ray photoelectron

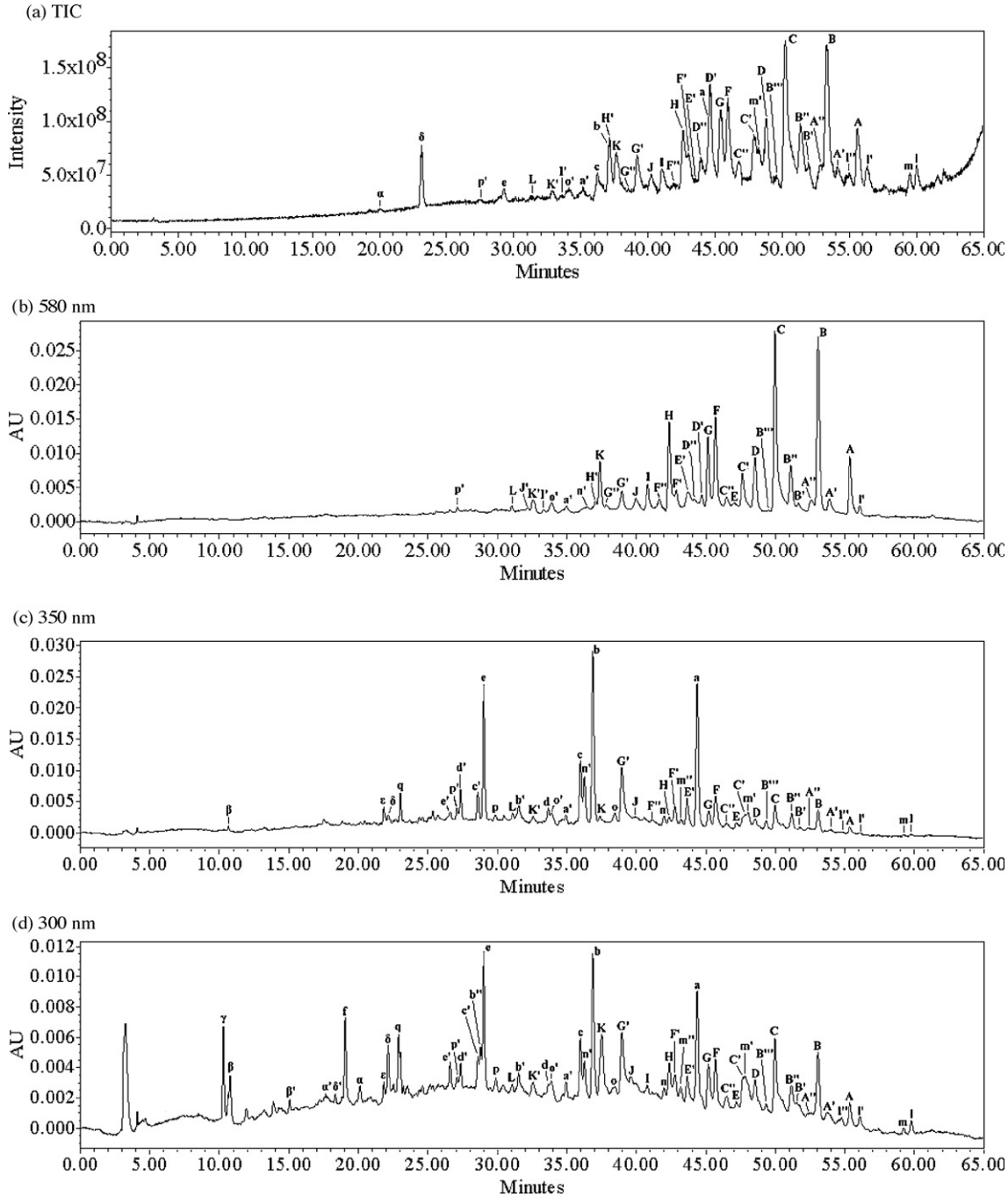

Fig. 8. (a) Total ion chromatogram and HPLC chromatogram of the photocatalytic degradation intermediates in F-TiO_2 (1.0 g L^{-1}) aqueous with 8 h of irradiation, at pH 9, recorded at (b) 580 nm, (c) 350 nm, and (d) 300 nm.

spectroscopy (HRXPS). An HRXPS measurement was carried out with an ULVAC-PHI XPS:PHI Quantera SXM microprobe to measure the change in the surface structure after the reflux treatment. The Mg Kα radiation was generated with a voltage of 8 kV and current of 30 mA. The spectra were taken for each sample after Ar^+ (3 keV) sputter cleaning. Surface charging was minimized by spraying low energy electrons over the sample surface using a neutralizer gun. Binding energy spectra were recorded in the regions of C 1s, Ti 2p, O 1s, and F 1s. The binding energies of all peaks were referenced to the C 1s line (284.6 eV) originating from surface impurity carbons.

2.3.2. Analyses of intermediates

The original dye and its intermediates of photocatalytic degradation were separated and identified by HPLC–PDA-ESI-MS. The HPLC–PDA-ESI-MS system consisted of a Waters 1525 binary pump, a 2996 photodiode array detector, an 717 plus) autosampler, a ZQ4000 micromass detector, and an Atlantis™ dC18 column (250 mm × 4.6 mm i.d., dp = 5 μm). The flow rate of the mobile phase was set at 1.0 mL min^{-1}. A linear gradient was set as follows: $t = 0$, $A = 95$, $B = 5$; $t = 20$, $A = 50$, $B = 50$; $t = 40$–45, $A = 10$, $B = 90$; $t = 48$, $A = 95$, $B = 5$. The column effluent was introduced into the ESI source of the mass spectrometer. Sixty-two intermediates of the process were separated and identified. The mineralization of the dye was monitored by measuring the total organic carbon (TOC) content with a Tekmar-Dohrmann Phoenix 8000 TOC Analyzer by directly injecting the aqueous solution.

3. Results and discussion

3.1. Characterization of catalyst

XRD pattern (Fig. 1S of supporting information) of catalysts can be readily indexed to the P25-TiO_2 phase (JCPDS card no. 36-1451). No obvious characteristic peaks are observed for other

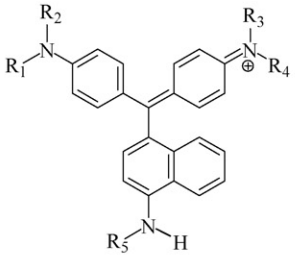

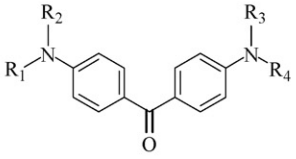

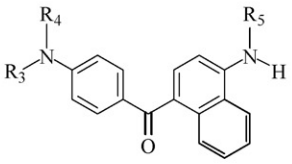

A : VBR, $R_{1\text{-}4} = CH_3$, $R_5 = C_2H_5$
B : $R_{1\text{-}3} = CH_3$, $R_4 = H$, $R_5 = C_2H_5$
C : $R_{1\text{-}2} = CH_3$, $R_{3\text{-}4} = H$, $R_5 = C_2H_5$
D : $R_1 = R_3 = CH_3$, $R_2 = R_4 = H$, $R_5 = C_2H_5$
E : $R_{1\text{-}4} = CH_3$, $R_5 = H$
F : $R_1 = CH_3$, $R_{2\text{-}4} = H$, $R_5 = C_2H_5$
G : $R_{1\text{-}3} = CH_3$, $R_4 = H$, $R_5 = H$
H : $R_{1\text{-}4} = H$, $R_5 = C_2H_5$
I : $R_{1\text{-}2} = CH_3$, $R_{3\text{-}4} = H$, $R_5 = H$
J : $R_1 = R_3 = CH_3$, $R_2 = R_4 = H$, $R_5 = H$
K : $R_1 = CH_3$, $R_{2\text{-}4} = H$, $R_5 = H$
L : $R_{1\text{-}5} = H$
A' : $R_{1\text{-}3} = CH_3$, $R_4 = CH_2OH$, $R_5 = C_2H_5$
A'' : $R_{1\text{-}4} = CH_3$, $R_5 = CHOHCH_3$
B' : $R_{1\text{-}2} = CH_3$, $R_3 = CH_2OH$, $R_4 = H$, $R_5 = C_2H_5$
B'' : $R_1 = R_3 = CH_3$, $R_2 = CH_2OH$, $R_4 = H$, $R_5 = C_2H_5$
B''' : $R_{1\text{-}3} = CH_3$, $R_4 = H$, $R_5 = CHOHCH_3$
C' : $R_1 = CH_3$, $R_2 = CH_2OH$, $R_{3\text{-}4} = H$, $R_5 = C_2H_5$
C'' : $R_{1\text{-}2} = CH_3$, $R_{3\text{-}4} = H$, $R_5 = CHOHCH_3$
D' : $R_1 = CH_3$, $R_2 = R_4 = H$, $R_3 = CH_2OH$, $R_5 = C_2H_5$
D'' : $R_1 = R_3 = CH_3$, $R_2 = R_4 = H$, $R_5 = CHOHCH_3$
E' : $R_{1\text{-}3} = CH_3$, $R_4 = CH_2OH$, $R_5 = H$
F' : $R_1 = CH_2OH$, $R_{2\text{-}4} = H$, $R_5 = C_2H_5$
F'' : $R_1 = CH_3$, $R_{2\text{-}4} = H$, $R_5 = CHOHCH_3$
G' : $R_{1\text{-}2} = CH_3$, $R_3 = CH_2OH$, $R_{4\text{-}5} = H$
G'' : $R_1 = R_3 = CH_3$, $R_2 = CH_2OH$, $R_{4\text{-}5} = H$
H' : $R_{1\text{-}4} = H$, $R_5 = CHOHCH_3$
I' : $R_1 = CH_3$, $R_2 = CH_2OH$, $R_{3\text{-}5} = H$
J' : $R_1 = CH_3$, $R_2 = R_{4\text{-}5} = H$, $R_3 = CH_2OH$
K' : $R_1 = CH_2OH$, $R_{2\text{-}5} = H$

a : $R_{1\text{-}4} = CH_3$
b : $R_{1\text{-}3} = CH_3$, $R_4 = H$
c : $R_{1\text{-}2} = CH_3$, $R_{3\text{-}4} = H$
d : $R_1 = R_3 = CH_3$, $R_2 = R_4 = H$
e : $R_1 = CH_3$, $R_{2\text{-}4} = H$
f : $R_{1\text{-}4} = H$
a' : $R_{1\text{-}3} = CH_3$, $R_4 = CH_2OH$
b' : $R_{1\text{-}2} = CH_3$, $R_3 = CH_2OH$, $R_4 = H$
b'' : $R_1 = R_3 = CH_3$, $R_2 = CH_2OH$, $R_4 = H$
c' : $R_1 = CH_3$, $R_2 = CH_2OH$, $R_{3\text{-}4} = H$
d' : $R_1 = CH_3$, $R_2 = R_4 = H$, $R_3 = CH_2OH$
e' : $R_1 = CH_2OH$, $R_{2\text{-}4} = H$

l : $R_{3\text{-}4} = CH_3$, $R_5 = C_2H_5$
m : $R_3 = CH_3$, $R_4 = H$, $R_5 = C_2H_5$
n : $R_{3\text{-}4} = H$, $R_5 = C_2H_5$
o : $R_{3\text{-}4} = CH_3$, $R_5 = H$
p : $R_3 = CH_3$, $R_{4\text{-}5} = H$
q : $R_{3\text{-}5} = H$
l' : $R_3 = CH_3$, $R_4 = CH_2OH$, $R_5 = C_2H_5$
l'' : $R_{3\text{-}4} = CH_3$, $R_5 = CHOHCH_3$
m' : $R_3 = CH_2OH$, $R_4 = H$, $R_5 = C_2H_5$
m'' : $R_3 = CH_3$, $R_4 = H$, $R_5 = CHOHCH_3$
n' : $R_{3\text{-}4} = H$, $R_5 = CHOHCH_3$
o' : $R_3 = CH_3$, $R_4 = CH_2OH$, $R_5 = H$
p' : $R_3 = CH_2OH$, $R_{4\text{-}5} = H$

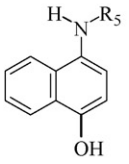

? : $R_5 = C_2H_5$
? : $R_5 = H$
?' : $R_5 = CHOHCH_3$

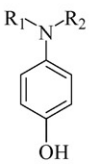

? : $R_{1\text{-}2} = CH_3$
? : $R_1 = CH_3$, $R_2 = H$
? : $R_{1\text{-}2} = H$
?' : $R_1 = CH_3$, $R_2 = CH_2OH$
?' : $R_1 = CH_2OH$, $R_2 = H$

Fig. 9. Chemical structure of photodecomposed intermediates.

impurities. Further observation showed that the peak intensities of modified-TiO_2 became weaker, indicating reduced crystallization. Fig. 2 shows XPS survey spectra of TiO_2, F-TiO_2, and Nafion-TiO_2 powder. The intensity of F 1s in Nafion-TiO_2 is strong, and that in F-TiO_2 is very weak. The F 1s peak originated from the surface fluoride (≡Ti–F) formed by a ligand exchange between F^- and the surface hydroxyl group on TiO_2. The F-TiO_2 and Nafion-TiO_2 samples clearly show the peak of F 1s as well as those of Ti, O, and C elements. For F-TiO_2, the F 1s binding energy (BE) of 683.2 eV in this spectrum b (Fig. 2S) corresponds to that of F^- adsorbed on TiO_2 (physically adsorbed F^- or F that replaces surface hydroxyl groups), and no sign of F ions in the lattice (BE = 688.5 eV) was found [30]. For Nafion-TiO_2, only one F 1s peak (peak 1) at 689.2 eV was observed (spectrum a), and this is attributed to F bonding on the carbon of polymer [16]. The surface morphology of the TiO_2, F-TiO_2, and Nafion-TiO_2 catalysts were examined with a FESEM (Fig. 3S of supporting information).

3.2. Control experiments

To confirm the role of Nafion-TiO_2 and F-TiO_2 in the photocatalytic reaction, three sets of experiments were performed to compare VBR degradation rates with and without catalysts at pH 9. One set was performed with VBR (0.05 g L^{-1}) exposed to TiO_2 or F-TiO_2 or Nafion-TiO_2 (0.5 g L^{-1}) but no UV (the catalyst-only condition). The second set was performed by exposing VBR (0.05 g L^{-1}) to UV without catalyst (the photolysis condition). Then, the third set was performed by exposing VBR to catalyst (0.5 g L^{-1}) in the presence of UV irradiation (the photocatalytic condition). The results are presented in Fig. 3. First, the experiment with TiO_2 or F-TiO_2 or Nafion-TiO_2 only showed that a small amount of VBR (about 7%, 15%, 24%) was adsorbed on the catalyst surface. Next, the results of the photolysis and photocatalytic experiments showed that the photolysis reaction resulted in a 2.1% decrease in the VBR concentration after 8 h while the VBR was 82.4%, 93.1%, and 96.8% removed after 3 h in the case of the photocatalytic reaction with TiO_2 or F-TiO_2 or Nafion-TiO_2, respectively. Fig. 3 compares the photocatalytic degradation of VBR among P25 TiO_2, F-TiO_2, and Nafion-TiO_2 systems, Nafion-TiO_2 induced faster photocatalytic degradation of VBR than did F-TiO_2 and P25 TiO_2. The presence of NaF or Nafion deposits led to a positive effect in the removal rate of VBR. Over 99% of the VBR was removed within 5 h of irradiation in all cases.

3.3. pH effect

The photodegradation efficiency and kinetics of the VBR with TiO_2 or F-TiO_2 or Nafion-TiO_2 as a function of reaction pH is shown in Fig. 4. As expected, the rate constant of the VBR dye was found to increase with the increase in pH value. The increase of adsorption of VBR on Nafion-TiO_2 in alkaline solutions was attributed to the increased difference of zeta potential between positively charged VBR and negatively charged Nafion-TiO_2 in alkaline solutions. It is known from Beer's law that normalized concentration of the solution equals normalized maximum absorbance, so we use C_0/C to take the place of A_0/A. Clearly, the photodegradation of VBR catalyzed by the TiO_2 or F-TiO_2 or Nafion-TiO_2 fits the pseudo first-order reaction well, i.e., $\ln(C_0/C) = k_{app}t$, where C_0 and C are the

Table 1
Identification of the N-de-alkylated intermediates from the photocatalytic degradation of VBR by HPLC–ESI-MS.

TIC peaks	Intermediates	[M+H^+]	ESI-MS spectrum (m/z) ions	Absorption maximum (nm)
A	Bis(4-dimethylaminophenyl)(4-ethylaminonaphthenyl)methylium	422.62	393.57, 334.62, 301.40	608.9, 590.5
B	(4-Dimethylaminophenyl)(4-methylaminophenyl) (4-ethylaminonaphthyl)methylium	408.48	379.49, 301.40	606.5, 567.3
C	(4-Dimethylaminophenyl)(4-aminophenyl) (4-ethylaminonaphthyl)methylium	394.59	365.53, 287.45, 258.58	604.0, 558.7
D	(4-Methylaminophenyl)(4-methylaminophenyl) (4-ethylaminonaphthyl)methylium	394.72	365.47, 301.59, 273.43	611.4, 558.7
E	(4-Dimethylaminophenyl)(4-dimethylaminophenyl) (4-aminonaphthyl)methylium	394.15	365.08, 349.19, 257.94	598.6, 566.0
F	(4-Methylaminophenyl)(4-aminophenyl) (4-ethylaminonaphthyl)methylium	380.51	335.58, 273.37	597.9
G	(4-Dimethylaminophenyl) (4-methylaminophenyl) (4-aminonaphthyl)methylium	380.45	351.52, 287.58, 209.23	607.7, 541.6
H	(4-Aminophenyl)(4-aminophenyl) (4-ethylaminonaphthyl)methylium	366.43	259.48	586.9
I	(4-Dimethylaminophenyl)(4-aminophenyl) (4-aminonaphthyl)methylium	366.23	307.23, 273.37, 245.53	575.8
J	(4-Methylaminophenyl) (4-methylaminophenyl) (4-aminonaphthyl)methylium	366.62	338.27, 273.62, 244.44	558.2
K	(4-Methylaminophenyl)(4-aminophenyl) (4-aminonaphthyl)methylium	352.29	293.59, 245.46	548.2,
L	(4-Aminophenyl)(4-aminonaphthyl)methylium	338.40	305.50, 245.40, 217.49	541.6
A′	(4-Hydroxymethylmethylaminophenyl) (4-dimethylmethylaminophenyl) (4-ethylaminonaphthyl)methylium	438.69	409.70, 379.55, 317.53	655.6, 580.7
A″	Bis(4-dimethylaminophenyl)(4-hydroxyethylaminonaphthyl)methylium	438.56	365.47, 333.60, 301.34	653.1
B′	(4-Hydroxymethylaminophenyl) (4-methylaminophenyl) (4-ethylaminonaphthyl)methylium	424.74	364.51, 301.59	658.0
B″	(4-Dimethylaminophenyl) (4-hydroxymethylaminophenyl) (4-ethylaminonaphthyl)methylium	424.54	395.30, 303.45, 274.46	627.3, 563.6
B‴	(4-Dimethylaminophenyl) (4-methylaminophenyl) (4-hydroxyethylaminonaphthyl)methylium	424.48	395.49, 317.47, 288.41	628.6, 563.6
C′	(4-Hydroxymethylmethylaminophenyl) (4-aminophenyl) (4-ethylaminonaphthyl)methylium	410.72	381.41, 303.39, 212.50	626.1, 559.9
C″	(4-Dimethylaminophenyl)(4-aminophenyl) (4-hydroxyethylaminonaphthyl)methylium	410.53	381.54, 303.39, 274.58	620.8, 542.8
D′	(4-Hydroxymethylaminophenyl) (4-methylaminophenyl) (4-ethylaminonaphthyl)methylium	410.66	380.45, 321.44, 273.43	594.2
D″	(4-Methylaminophenyl) (4-methylaminophenyl) (4-hydroxyethylaminonaphthyl)methylium	410.53	381.54, 317.53, 273.62	599.1, 534.3
E′	(4-Hydroxymethylaminophenyl) (4-dimethylaminophenyl) (4-aminonaphthyl)methylium	410.40	365.47, 273.37, 220.43	595.4, 557.5
F′	(4-Hydroxymethylaminophenyl) (4-aminophenyl) (4-ethylaminonaphthyl)methylium	396.64	351.58, 326.56, 274.58	554.0, 337.0
F″	(4-Methylaminophenyl)(4-aminophenyl) (4-hydroxyethylaminonaphthyl)methylium	396.51	353.50, 303.32, 274.58	585.6
G′	(4-Hydroxymethylmethylaminophenyl) (4-methylaminophenyl) (4-aminonaphthyl)methylium	396.53	367.39, 301.53, 244.57	584.4
G″	(4-Dimethylaminophenyl) (4-hydroxymethylaminophenyl) (4-aminonaphthyl)methylium	396.45	367.71, 289.43, 214.16	596.7
H′	(4-Aminophenyl)(4-aminophenyl) (4-hydroxyethylaminonaphthyl)methylium	382.43	323.29, 275.22, 225.56	594.2
I′	(4-Hydroxymethylmethylaminophenyl) (4-aminophenyl) (4-aminonaphthyl)methylium	382.53	321.31, 293.53, 245.46	593.9
J′	(4-Hydroxymethylaminophenyl) (4-methylaminophenyl) (4-aminonaphthyl)methylium	N/A	N/A	591.2
K′	(4-Hydroxymethylaminophenyl) (4-aminophenyl) (4-aminonaphthyl)methylium	368.54	338.64, 245.14, 215.44	590.5, 333.4

initial and actual concentrations of VBR, respectively, and k_{app} is the apparent rate constant of the degradation.

Under acidic conditions, it was found difficult to adsorb the cationic VBR dye onto the TiO_2 or F-TiO_2 or Nafion-TiO_2 surface. The active •OH radicals, formed in low concentrations, and hence the photodegradation process of VBR remained slow. With higher pH values, the formation of active •OH species is favored, due to not only improved transfer of holes to the adsorbed hydroxyls, but also electrostatic abstractive effects between the negatively charged TiO_2 or F-TiO_2 or Nafion-TiO_2 particles and the operating cationic dyes. Although the VBR dye can adsorb onto the TiO_2 or F-TiO_2 or Nafion-TiO_2 surface to some extent in alkaline media, when the pH value is too high (pH 11), the VBR dye molecules will change to a leuco-compound [31]. Our results indicate that the F-TiO_2 or Nafion-TiO_2 surface is negatively charged, and the VBR adsorbs onto the F-TiO_2 or Nafion-TiO_2 surface through the positive ammonium groups. We can conclude from Fig. 4 that the degradation of VBR in aqueous solution catalyzed by Nafion-TiO_2 was faster than that catalyzed by the P-25 TiO_2 and F-TiO_2 and that this conclusion held true at different pH values. In the following experiment, we chose pH 9 as the optimum condition.

3.4. Effect of NaF or Nafion polymer concentration

The photoactivity of the sample was strongly dependent on the amount of NaF. With NaF increasing from 0.42 to 0.84 g/g of TiO_2, the photoactivity of the sample for the RhB photodegradation was enhanced. With the exclusion of the sample, the as-prepared samples showed higher photoactivities for the VBR degradation than did P25-TiO_2. The maximum photoactivity was observed for the sample NaF = 0.84 g. When NaF was boosted to 2.10 g, the photoactivity of the sample decreased, which is in agreement with the literature [24]. Although it presented a surface area (51.3 m^2/g) similar to that of the samples 48.2 m^2/g and 0.84 g NaF, the photocatalytic activity was fairly different. Therefore, it was inferred that specific surface areas played a minor role in this photocatalytic process.

To investigate the relation between Nafion polymer concentration on photocatalyst and degradation of VBR (cationic dye), the amount of Nafion polymer solution was varied between 0 and 2.0 mL in a series of experiments under constant process conditions: dye concentration = 50 mg L^{-1}. Fig. 5 shows curves of degraded dye for various catalyst loadings at pH 9. As expected, the photodegradation rate of the VBR was found to increase then decrease with the increase in the Nafion polymer concentration. The coating of 2.0 mL of 5 wt% Nafion per gram of TiO_2 was enough to reduce slightly the photocatalytic rate, which might decrease the adsorption and produce a hydrophobic surface. The presence of the optimum Nafion deposits (1.0 mL) led to a positive effect in the removal rate of VBR. Upon adding Nafion to the aqueous suspension, zeta potentials became negative over the entire pH range, which is in agreement with the literature value [22]. The negative shift of zeta potentials was larger with higher Nafion concentration. This should be ascribed to the fact that the anionic sulfonate groups (–SO_3–) in the Nafion layer outnumber the positively charged surface functional groups on TiO_2 (≡$TiOH_2^+$). The surface charge modified by Nafion adlayers directly influences the electrostatic interaction between charged substrates and the catalyst surface. Negatively charged molecules should be repelled from the surface of Nafion-TiO_2 while positively charged ones should be attracted. In Choi and co-worker report [22], the visible-light-sensitized degradation of dyes was enhanced with Nafion-TiO_2 not only for cationic dyes (methylene blue and rhodamine B) whose uptake on Nafion-TiO_2 is enhanced, but also for an anionic dye (acid organic 7) that is adsorbed on Nafion-TiO_2.

Table 2
Identification of intermediates of the destruction of the conjugated structure of the VBR dye by HPLC–PDA-ESI-MS.

HPLC peaks	Intermediates	[M+H$^+$]	ESI-MS spectrum (m/z) ions	Absorption maximum (nm)
a	4-(*N*,*N*-Dimethylamino)-4′-(*N*′,*N*′-dimethylamino)benzophenone	269.31	230.21	369.1
b	4-(*N*,*N*-Dimethylamino)-4′-(*N*′-methylamino)benzophenone	255.51	223.31	366.7
c	4-(*N*-Methylamino)-4′-(*N*′-methylamino)benzophenone	241.24	N/A	363.1
d	4-(*N*,*N*-Dimethylamino)-4′-aminobenzophenone	N/A	N/A	365.5
e	4-(*N*-Methylamino)-4′-aminobenzophenone	227.28	201.10	357.2
f	4,4′-Bis-aminobenzophenone	N/A	N/A	331.0
a′	4-(*N*,*N*-Dimethylamino)-4′-(*N*′-hydroxymethyl-*N*′-methylamino)benzophenone	285.47	232.21	364.3
b′	4-(*N*-Hydroxymethyl-*N*-methylamino)-4′-(*N*′-methylamino)benzophenone	N/A	N/A	341.8
b″	4-(*N*,*N*-Dimethylamino)-4′-(*N*′-hydroxymethylamino)benzophenone	N/A	N/A	357.2
c′	4-(*N*-Methylamino)-4′-(*N*′-hydroxymethylamino)benzophenone	N/A	N/A	353.8
d′	4-(*N*-Hydroxymethyl-*N*-methylamino)-4′-aminobenzophenone	N/A	N/A	359.1
e′	4-(*N*-Hydroxymethylamino)-4′-aminobenzophenone	243.22	N/A	347.8
l	4-(*N*,*N*-Dimethylaminophenyl)-4′-(*N*′-ethylaminonaphthyl)ketone	319.52	289.56, 272.34, 226.45	375.2
m	4-(*N*-Methylaminophenyl)-4′-(*N*′-ethylaminonaphthyl)ketone	305.21	244.89	366.7
n	4-(Aminophenyl)-4′-(*N*′-ethylaminonaphthyl)ketone	N/A	N/A	339.1
o	4-(*N*,*N*-Dimethylaminophenyl)-4′-(aminonaphthyl)ketone	N/A	N/A	345.4
p	4-(*N*-Methylaminophenyl)-4′-(aminonaphthyl)ketone	N/A	N/A	343.0
q	4-(Aminophenyl)-4′-(aminonaphthyl)ketone	N/A	N/A	331.0
l′	4-(*N*-Hydroxymethyl-*N*-methylaminophenyl)-4′-(*N*′-ethylaminonaphthyl)ketone	335.64	301.59, 270.04, 237.20	377.6
l″	4-(*N*,*N*-Dimethylaminophenyl)-4′-(*N*′-hydroxyethylaminonaphthyl)ketone	335.58	289.18, 259.41, 244.50	373.5
m′	4-(*N*-Hydroxymethylaminophenyl)-4′-(*N*′-ethylaminonaphthyl)ketone	321.10	233.95	367.9
m″	4-(*N*-Methylaminophenyl)-4′-(*N*′-hydroxyethylaminonaphthyl)ketone	N/A	N/A	371.6
n′	4-(Aminophenyl)-4′-(*N*′-hydroxyethylaminonaphthyl)ketone	N/A	N/A	356.2
o′	4-(*N*-Hydroxymethyl-*N*-methylaminophenyl)-4′-(aminonaphthyl)ketone	307.61	279.58, 252.63, 206.23	363.1
p′	4-(*N*-Hydroxymethylaminophenyl)-4′-(aminonaphthyl)ketone	293.59	265.56	343.0
α	4-(*N*,*N*-Dimethylamino)phenol	138.84	108.31	260.7
α′	4-(*N*-Hydroxymethyl-*N*′-methylamino)phenol	N/A	N/A	271.2
β	4-(*N*-Methylamino)phenol	N/A	N/A	250.0
β′	4-(*N*-Hydroxymethylamino)phenol	N/A	N/A	245.3
γ	4-Aminophenol	N/A	N/A	247.7
δ	4-(*N*-Ethylamino)naphthenol	188.93	149.19, 108.03	288.1
δ′	4-(*N*-Hydroxyethylamino)naphthenol	N/A	N/A	289.2
ε	4-(Amino)naphthenol	N/A(160)	N/A	271.4

3.5. Evolution of TOC

The complete mineralization of 1 mol of VBR dye molecules implies the formation of an equivalent amount (29 mol) of CO_3^{2-} at the end of the treatment. However, the depletion in TOC (shown in Fig. 6) clearly indicates that the reaction did not go to completion. In fact, after 24 h irradiation, about 71.4%, 86.1%, and 93.8% (for P25-TiO_2, F-TiO_2, and Nafion-TiO_2) of the initial organic carbon had been transformed into CO_2, implying the continued existence of other organic compounds in the irradiated solution. These findings are in agreement with those obtained in a study concerning the photocatalytic degradation of basic violet 4 [32], in which the persistence of various aromatic compounds was reported even after long-term irradiation.

3.6. Evolution of UV–vis spectra

The absorption spectra of the solutions during irradiation catalyzed by the two kinds of catalysts are illustrated in Fig. 7. The degradation processes are different as seen from a comparison

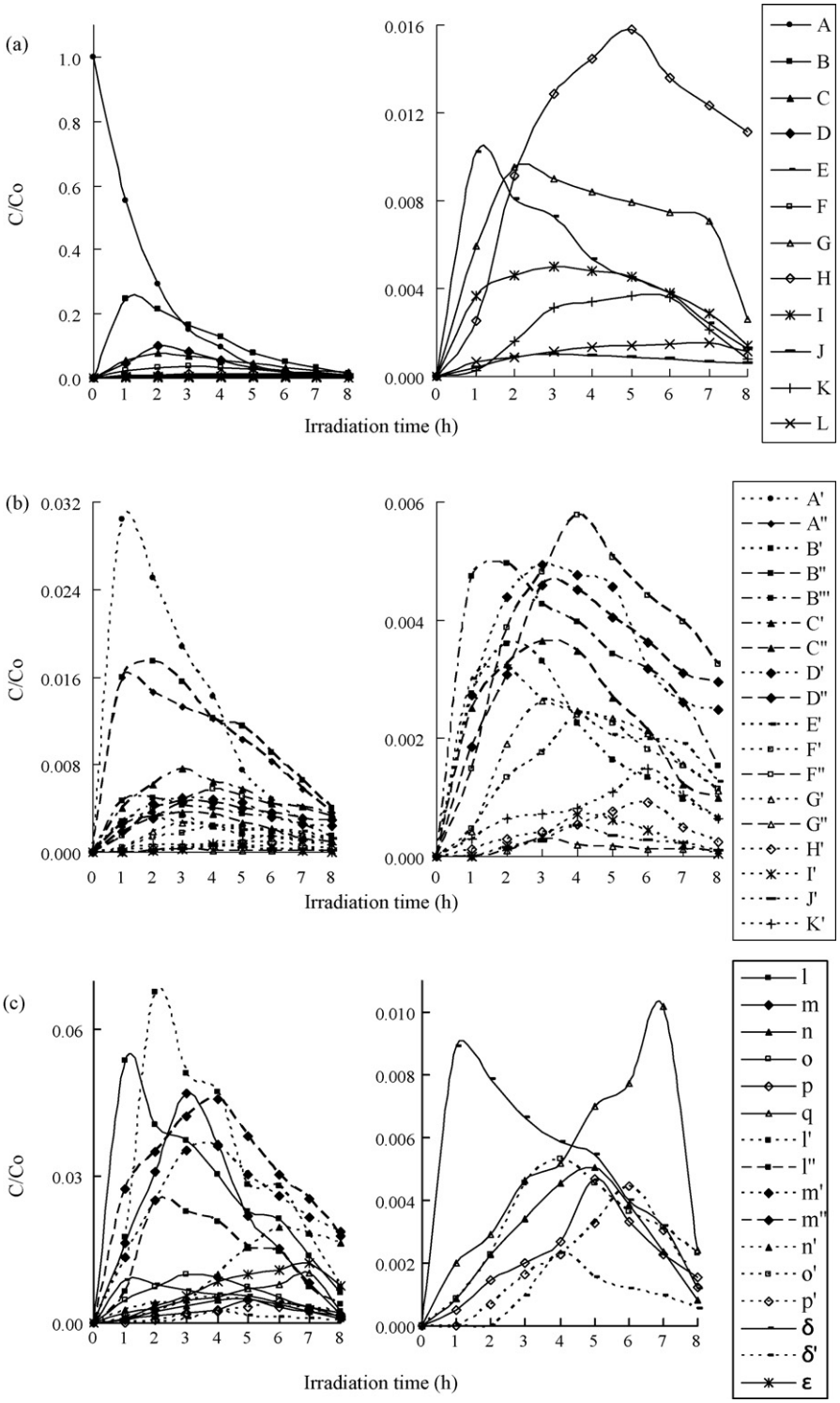

Fig. 10. Variation in the relative distribution of the intermediates obtained from the photodegradation of the VBR dye as a function of the irradiation time. (a) Curves A–L, (b) curves A′–K′, (c) curves l–q, l′–p′, δ–ε, δ′, and (d) curves a–f, a′–e′, α–γ, α′–β′, correspond to peaks **A–L**, **A′–K′**, **a–f**, **a′–e′**, **l–q**, **l′–p′**, **α–ε** and **α′–δ′** in Fig. 8, respectively.

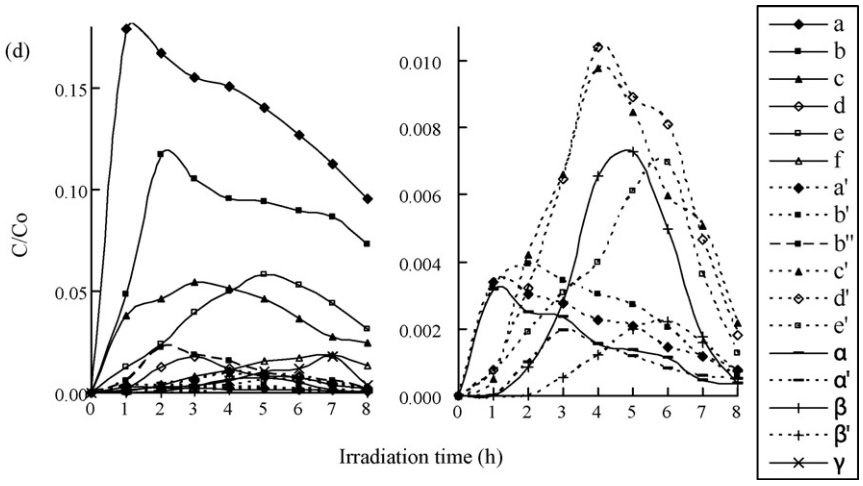

Fig. 10. (*Continued*).

of Fig. 7a and b. When assisted by F-TiO_2, in addition to the fast decay in absorbance of VBR solution, a blue shift in the absorbance maximum was observed at the same time. After illumination for 6 h, the absorbance peak shifted from 609.8 to 591.3 nm, which indicated that the *N*-de-ethylation and cleavage of the VBR chromophore ring structure may have been occurred at the same time. This is coincident with our results [33], and we have attributed the peak shift to the *N*-de-ethylation of Acid Blue 1 with the help of HPLC. As seen from Fig. 7b, the shift of the absorption peak was too small to be noticed. Assisted by the Nafion-TiO_2, only a gradually decrease of the maximum absorbance of the solution can be observed, and no new peaks appeared, indicating that cleavage of the VBR chromophore ring structure was the only event. These results suppose that when the F-TiO_2 surface is negatively charged, the VBR (cationic dye) adsorbs onto it through the positive diethylamino groups. When the Fluorine atom of Nafion layer on TiO_2 surface is high electronegativity, the VBR adsorbs onto it through the conjugated structure (electron rich) (inset of Fig. 7). A similar effect on the F-TiO_2 and Nafion-TiO_2 surface adsorption and photocatalytic reaction has been reported for the degradation of organic compounds [11,16–19]. In Fig. 7a and b, it was also found that the absorbance decreased from 1.24 to 1.16 AU (1.24 to 0.62 AU). The former was in the initial dye concentration while the latter was in the 100 mL solution to which 0.05 g F-TiO_2 (Nafion-TiO_2) was added. After UV irradiation for 6 h, ca. 96.5% (99.9%) of the VBR dye was degraded. The result showed that the cationic dye VBR could easily adsorb on the F-TiO_2 and Nafion-TiO_2 surfaces, and hence the photodegradation efficiencies were fast.

3.7. Degradation mechanisms of VBR

Total ion chromatograms were obtained for an irradiated VBR solution after 8 h, at pH 9, with UV light in the presence of F-TiO_2 ($1.0\,g\,L^{-1}$). These chromatograms, recorded at 580 nm, 350 nm, and 300 nm, are illustrated in Fig. 8a–d. With irradiation up to 8 h, 62 components are identified, all with the retention times of less than

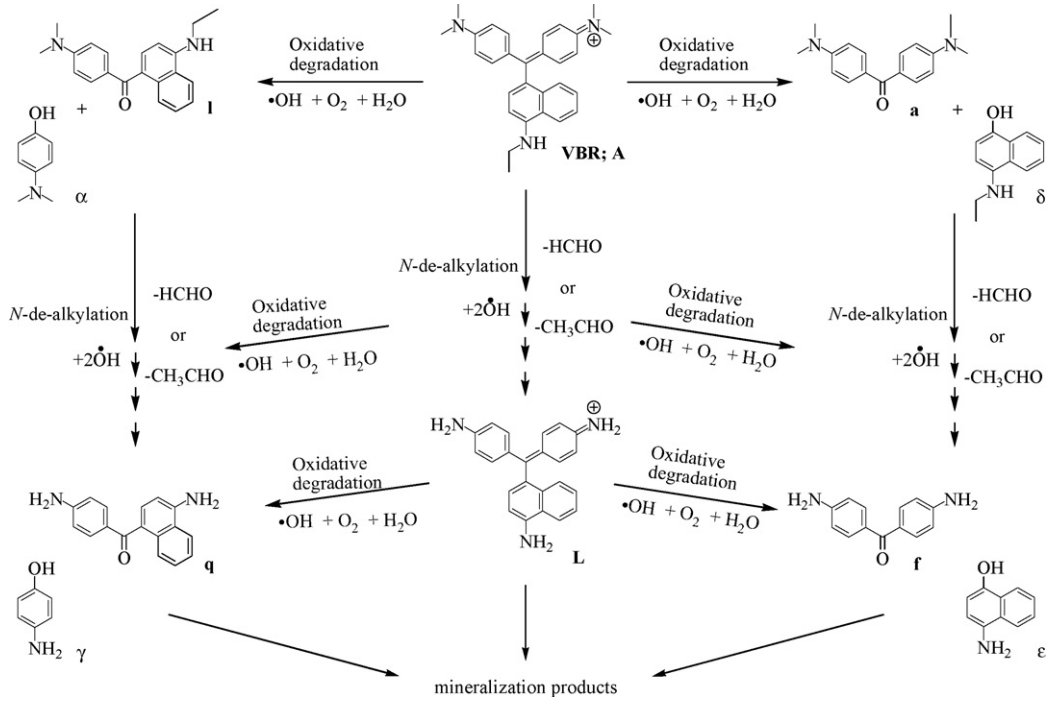

Fig. 11. Proposed mechanisms based on identification of intermediates formed chronologically during the photodegradation of VBR dye by HPLC–ESI-MS.

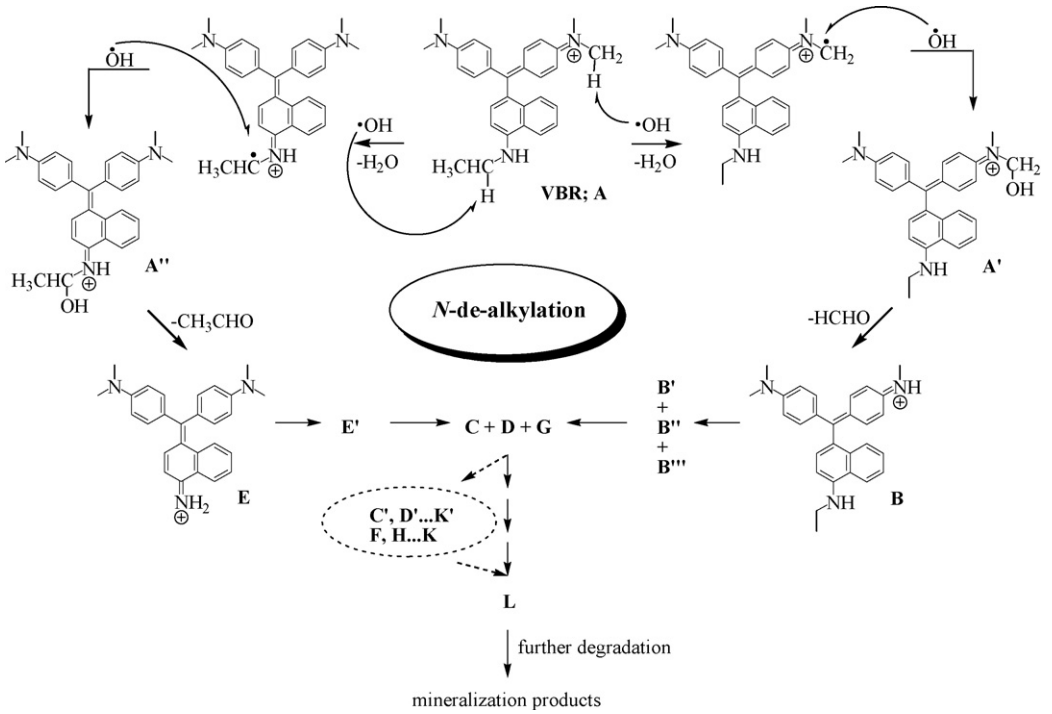

Fig. 12. Proposed *N*-de-alkylation pathway of the VBR dye following the identification of intermediates by HPLC–ESI-MS.

65 min. Several categories of intermediates can be distinguished in Fig. 9. We denoted the VBR dye and its related intermediates as species **A–L**, **A′–K′**, **a–f**, **a′–e′**, **l–q**, **l′–p′**, **α–γ**, **α′–β′**, **δ–ε**, and **δ′**. However, with Nafion-TiO_2, as catalyst, we only observed its related intermediates as species, **a–f**, **a′–e′**, **l–q**, **l′–p′**, **α–γ**, **α′–β′**, **δ–ε**, and **δ′**. The maximum absorption band of each intermediate in the visible and ultraviolet spectral region in Fig. 4S of supporting information and Tables 1 and 2 was measured, and these bands correspond to the peaks in Fig. 8, respectively. The intermediates were further identified using the HPLC–ESI mass spectrometric method; the relevant mass spectra are illustrated in Fig. 5S of the supporting information and Tables 1 and 2. The molecular ion peaks appeared to be in the acid forms of the intermediates. The concentration of the other intermediates may be under the detection limit. The intermediates identified in this study, **a–f** and **α–γ**, were also identified in a previous study of the MG/TiO_2 system [31]. On the basis of all the above experimental results and the relative distribution of all of the intermediates obtained are illustrated in Fig. 10, we tentatively propose the dye degradation mechanism depicted in Fig. 11. During the initial period of VBR dye photodegradation by F-TiO_2, competitive reactions between *N*-de-alkylation and oxidative degradation (cleavage of the VBR chromophore ring structure) occurs based on the intermediates identified. Then, oxidation degradation occurs only by Nafion-TiO_2. The detailed mechanisms are illustrated in the following description.

3.7.1. *N*-de-alkylation of VBR

The relative distribution of all of the intermediates obtained is illustrated in Fig. 10a. The distributions of all of the *N*-de-alkylated

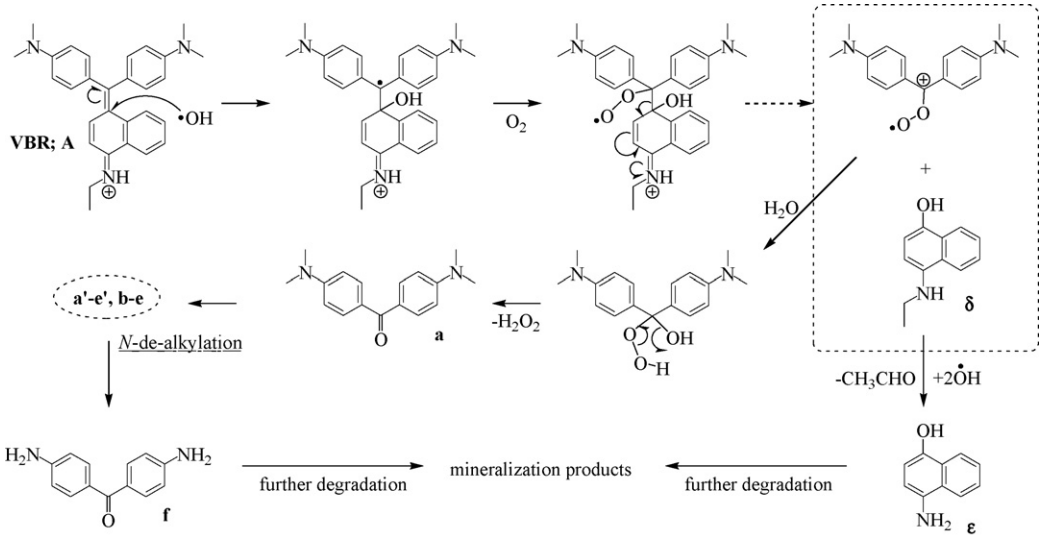

Fig. 13. Proposed oxidation pathway of the VBR dye.

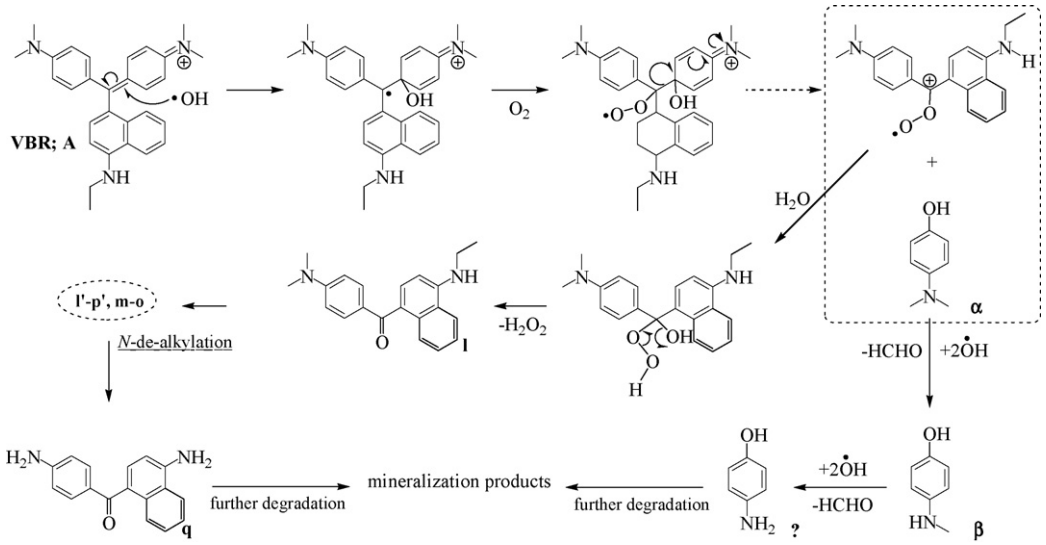

Fig. 14. Proposed oxidation pathway of the VBR dye.

and their hydroxylated intermediates are relative to the initial concentration of VBR. Nonetheless, we clearly observed the changes in the distribution of each intermediate during the photodegradation of VBR. Except for the initial VBR dye (peak A), the intensities of the peaks increased at first and subsequently decreased, indicating the formation and transformation of the intermediates. The successive appearance of the maximum of each intermediate indicates that the *N*-de-alkylation of VBR is a stepwise photochemical process by hydroxylated intermediates created.

The *N*-de-alkylation of the VBR occurs mostly through attack by the •OH species on the *N*,*N*-dimethyl group or *N*-ethyl group of VBR. In the hydroxylation of VBR, **A**′ or **A**″ reaches its maximum concentration after a 1-h irradiation period because of the •OH attack on the *N*,*N*-dimethyl group or *N*-ethyl group of VBR (curve A′ or A″). The *N*-mono-de-methylated intermediate, **B**, or the *N*-mono-de-ethylated intermediate, **E**, was clearly observed to reach its maximum concentration after a 1-h irradiation period (curve B or E), respectively. The other hydroxylated intermediates, **B**′–**G**″, were clearly observed (curve B′–G″) to reach their maximum concentration after a 2–3 h irradiation period. The other *N*-alkylated intermediates, **C**–**I**, were clearly observed (curve C–I) to reach their maximum concentration after a 2–3 h irradiation period. The concentrations of the other *N*-de-alkylated intermediates and hydroxylated intermediates may be too low to be examined by HPLC–PDA-ESI-MS.

The successive appearance of the maximal quantity of each intermediate indicates that the *N*-de-ethylation of VBR is a stepwise photochemical process by the hydroxylated intermediates created. VBR gets near the negatively charged TiO_2 particle surface via the positive dimethylamine or ethylamine group. The results discussed above can be seen more clearly from Fig. 12.

3.7.2. Oxidative degradation of the VBR

The oxidative degradation of the VBR dye occurs mostly through attack by the •OH species on the central carbon portion of VBR and produces two sets of intermediates, **a** and **δ** intermediates, and **l** and **α** intermediates. The evolutions of the initial dye concentration and of the identified intermediates were followed as a function of irradiation time. The result is displayed in Fig. 10b. The oxidative degradation of intermediates in the first set was clearly observed (curves a and δ) to reach their maximum concentrations at the same time after a 1-h irradiation period. In the hydroxylation of an intermediate, the intermediate **a**′ reached its maximum concentration after a 2-h irradiation period because of the •OH attack on the central carbon of VBR (curve a′). The other oxidative intermediates were clearly observed (curves b–f and ε) to reach their maximum concentrations after a 2–7-h irradiation period. The other hydroxylated intermediates, **b**′–**e**′, were clearly observed (curves b′–e′) to reach their maximum concentrations after a 2–6-h irradiation period. The concentration of the other oxidative intermediates may be under the detectable limit. The results we discussed above can be seen more clearly from Fig. 13.

The second set of intermediates were clearly observed (curves l and α) to reach their maximum concentrations at the same time after a 1-h irradiation period. In the hydroxylation of **l** intermediate, **l**′ and **l**″ intermediates reached their maximum concentration after a 2-h irradiation period because of the •OH attack on the central carbon of VBR (curves l′ and l″). The other intermediates were clearly observed (curves m–q and β–γ) to reach their maximum concentrations after an 3–7-h irradiation period, respectively. The other hydroxylated intermediates, **m**′–**p**′, were clearly observed (curves m′–p′) to reach their maximum concentrations after a 4–6 h irradiation period. The concentrations of the other intermediates may be under the detectable limit. The results we discussed above can be seen more clearly from Fig. 14.

According to earlier reports [31–34], the *N*-de-alkylation processes are preceded by the formation of a nitrogen-centered radical while oxidative degradation (destruction of dye chromophore structures) is preceded by the generation of a carbon-centered radical. Consistent with this, degradation of VBR must occur via three different pathways (two oxidative degradations and one *N*-de-alkylation) due to formation of different radicals (either a carbon-centered or nitrogen-centered radical). The •OH attack on the dye is known to yield a dye cationic radical. After this step, the cationic radical $Dye^{\bullet+}$ can undergo hydrolysis and/or use various deprotonation pathways, which in turn are determined by the different adsorption modes of VBR on the catalyst particle surface.

4. Conclusions

VBR dye can be successfully decolorized and degraded by F-TiO_2 or Nafion-TiO_2 under UV irradiation. The presence of NaF or Nafion deposits positively impacted the removal rate of VBR. The rate constant of the VBR dye was found to increase with the increase in pH value. Under alkaline conditions (pH 9), a 0.84 g NaF or 1 mL Nafion solution on P25-TiO_2 catalyzed the degradation of VBR (50 mg/L)

much more efficiently than pure P25-TiO_2. In fact, after 24 h of irradiation, about 71.4%, 86.1%, and 93.8% (for P25-TiO_2, F-TiO_2, and Nafion-TiO_2) of the initial organic carbon had been transformed into CO_2. Based on the successful separation, identification and characterizaion of the process intermediates, we propose *N*-dealkylation and oxidative degradation of the VBR dye takes place in the presence of F-TiO_2, but oxidation degradation of the VBR dye occurs only by Nafion-TiO_2 particles. The reaction mechanisms proposed in this study should shed some light on future application of the technology to the decolorization of dyes.

Acknowledgment

This research was supported by the National Science Council of the Republic of China (NSC 97-2113-M-438-002-MY2).

Appendix A. Supplementary data

Supplementary data associated with this article can be found, in the online version, at doi:10.1016/j.jhazmat.2009.09.094.

References

[1] M.A. Fox, M.T. Dulay, Heterogeneous photocatalysis, Chem. Rev. 93 (1993) 381–433.
[2] Ullmann's Encyclopedia of Industrial Chemistry. Part A27. Triarylmethane and Diarylmethane Dyes, 6th ed., Wiley-VCH, New York, 2001.
[3] D.M. Marmion, Handbook of U.S. Colorants, John Wiley & Sons, New York, 1991.
[4] M.S. Baptista, G.L. Indig, Effect of BS a binding on photophysical and photochemical properties of triarylmethane dyes, J. Phys. Chem. B 102 (1998) 4678–4688.
[5] B.P. Cho, T. Yang, L.R. Blankenship, J.D. Moody, M. Churchwell, F.A. Bebland, S.J. Culp, Synthesis and characterization of N-de-methylated metabolites of malachite green and Leucomalachite green, Chem. Res. Toxicol. 16 (2003) 285–294.
[6] D.R. Doerge, M.I. Churchwell, T.A. Gehring, Y.M. Pu, S.M. Plakas, Analysis of malachite green and metabolites in fish using liquid chromatography atomospheric pressure chemical ionization mass spectrometry, Rapid Commun. Mass Spectrom. 12 (1998) 1625–1634.
[7] S.J. Culp, P.W. Mellick, R.W. Trotter, K.J. Greenlees, R.L. Kodell, F.A. Beland, Synthesis and characterization of *N*-de-methylated metabolites of malachite green and leucomalachite green, Food Chem. Toxicol. 44 (2006) 1204–1212.
[8] L.M. Lewis, G.L. Indig, Effect of dye aggregation on triarylmethanemediated photoinduced damage of hexokinase and DNA, J. Photochem. Photobiol. B: Biol. 67 (2002) 139–148.
[9] A.L. Linsebigler, G.Q. Lu, J.T. Yates Jr., Photocatalysis on TiO_2 surfaces: principles, mechanisms, and selected results, Chem. Rev. 95 (1995) 735–758.
[10] M.R. Hoffman, S.T. Martin, W. Choi, W. Bahnemann, Environmental applications of semiconductor photocatalysis, Chem. Rev. 95 (1995) 69–96.
[11] Y. Xu, K. Lv, Z. Xiong, W. Leng, W. Du, D. Liu, X. Xue, Rate enhancement and rate inhibition of phenol degradation over irradiated anatase and rutile TiO_2 on the addition of NaF: new insight into the mechanism, J. Phys. Chem. C 111 (2007) 19024–19032.
[12] C. Minero, G. Mariella, V. Maurino, D. Vione, E. Pelizzetti, Change of adsorption modes of dyes on fluorinated TiO_2 and its effect on photocatalytic degradation of dyes under visible irradiation, Langmuir 16 (2000) 8964–8972.
[13] D. Li, H. Haneda, S. Hishita, N. Ohashi, K.N. Labhsetwar, Fluorine-doped TiO_2 powders prepared by spray pyrolysis and their improved photocatalytic activity for decomposition of gas-phase acetaldehyde, J. Fluorine Chem. 126 (2005) 69–77.
[14] K. Chiang, R. Amal, T. Tran, Photocatalytic oxidation of cyanide: kinetic and mechanistic studies, J. Mol. Catal. A: Chem. 193 (2003) 285–297.
[15] S.M. Vohra, S. Kim, W. Choi, Effects of surface fluorination of TiO_2 on the photocatalytic degradation of tetramethylammonium, J. Photochem. Photobiol. A: Chem. 160 (2003) 55–60.
[16] H. Park, W. Choi, Effects of TiO_2 surface fluorination on photocatalytic reactions and photoelectrochemical behaviors, J. Phys. Chem. B 108 (2004) 4086–4093.
[17] J. Tang, H. Quan, J. Ye, Photocatalytic properties and photoinduced hydrophilicity of surface-fluorinated TiO_2, Chem. Mater. 19 (2007) 116–122.
[18] M.S. Vohra, K. Tanaka, Enhanced photocatalytic activity of Nafion-coated TiO_2, Environ. Sci. Technol. 35 (2001) 411–415.
[19] Q. Wang, C.C. Chen, D. Zhao, W.H. Ma, J.C. Zhao, Change of adsorption modes of dyes on fluorinated TiO_2 and its effect on photocatalytic degradation of dyes under visible irradiation, Langmuir 24 (2008) 7338–7345.
[20] J. Lee, W.C.J. Yoon, Photocatalytic degradation of N-nitrosodimethylamine: mechanism, product distribution, and TiO_2 surface modification, Environ. Sci. Technol. 39 (2005) 6800–6807.
[21] H. Park, W. Choi, Visible-light-sensitized production of hydrogen using perfluorosulfonate polymer-coated TiO_2 nanoparticles: an alternative approach to sensitizer anchoring, Langmuir 22 (2006) 2906–2911.
[22] H. Park, W. Choi, Photocatalytic reactivities of Nafion-coated TiO_2 for the degradation of charged organic compounds under UV or visible light, J. Phys. Chem. B 109 (2005) 11667–11674.
[23] G. Huang, Y. Zhu, Enhanced photocatalytic activity of $ZnWO_4$ catalyst via fluorine doping, J. Phys. Chem. C 111 (2007) 11952–11958.
[24] H. Fu, S. Zhang, T. Xu, Y. Zhu, J. Chen, Photocatalytic degradation of RhB by fluorinated Bi_2WO_6 and distributions of the intermediate products, Environ. Sci. Technol. 42 (2008) 2085–2091.
[25] C. Heitner-Wirguin, Recent advances in perfluorinated ionomer membranes: structure, properties and applications, J. Membr. Sci. 120 (1996) 1–33.
[26] J. Wang, P. Liu, S. Wang, W. Han, X. Wang, X. Fu, Nanocrystalline zinc oxide in perfluorinated ionomer membranes: preparation, characterization, and photocatalytic properties, J. Mol. Catal. A: Chem. 273 (2007) 21–25.
[27] P.L. Shao, K.A. Mauritz, R.B. Moore, [Perfluorosulfonate ionomer]/[SiO_2–TiO_2] nanocomposites via polymer-in situ sol–gel chemistry: sequential alkoxide procedure, J. Polym. Sci. Part B: Polym. Phys. 34 (1996) 873–882.
[28] H.W. Rollins, F. Lin, J. Johnson, J.J. Ma, J.T. Liu, M.H. Tu, D.D. Des-Marteau, Y.P. Sun, Nanoscale cavities for nanoparticles in perfluorinated ionomer membranes, Langmuir 16 (2000) 8031–8036.
[29] C.C. Chen, C.S. Lu, F.D. Mai, C.S. Weng, Photooxidative N-de-ethylation of anionic triarylmethane dye (sulfan blue) in titanium dioxide dispersions under UV irradiation, J. Hazard. Mater. B 137 (2006) 1600–1607.
[30] J.C. Yu, J.G. Yu, W. Ho, Z. Jiang, L. Zhang, Effects of F-doping on the photocatalytic activity and microstructures of nanocrystalline TiO_2 powders, Chem. Mater. 14 (2002) 3808–3816.
[31] C.C. Chen, C.S. Lu, Mechanistic studies of the photocatalytic degradation of methyl green: an investigation of products of the decomposition processes, Environ. Sci. Technol. 41 (2007) 4389–4396.
[32] C.C. Chen, C.S. Lu, Photocatalytic degradation of Basic Violet 4: degradation efficiency, product distribution, and mechanisms, J. Phys. Chem. C 111 (2007) 13922–13932.
[33] C.C. Chen, H.J. Fan, J.L. Jan, Degradation pathways and efficiencies of Acid Blue 1 by photocatalytic reaction with ZnO nanopowder, J. Phys. Chem. C 112 (2008) 11962–11972.
[34] G. Liu, X. Li, J. Zhao, H. Hidaka, N. Serpone, Photooxidation pathway of sulforhodamine-B. Dependence on the adsorption mode on TiO_2 exposed to visible light radiation, Environ. Sci. Technol. 34 (2000) 3982–3990.